*Geophysical Research Letters*

Supporting Information for

# Future Atmospheric Rivers and Impacts on Precipitation: Overview of the ARTMIP Tier2 High-Resolution Global Warming Experiment

Christine A. Shields[1*], Ashley E. Payne[2,3*], Eric J. Shearer[4,], Michael F. Wehner[5], Travis A. O'Brien[6,7], Jonathan J. Rutz[8], L. Ruby Leung[9], F. Martin Ralph[10], Allison B. Marquardt Collow[11,12], Paul A. Ullrich[13], Qizhen Dong[14], Alexander Gershunov[10,], Helen Griffith[15], Bin Guan[16], Juan M. Lora[17], Mengqian Lu[14], Elizabeth McClenny[13], Kyle M. Nardi[18], Mengxin Pan[14], Yun Qian[9], Alexandre M. Ramos[19,20], Tamara Shulgina[10], Maximiliano Viale[21] Chandan Sarangi[9, 22], Ricardo Tomé[20], Colin Zarzycki[18]

*These authors contributed equally to this work

[1]Climate and Global Dynamics Laboratory, National Center for Atmospheric Research, Boulder, CO, 80302, USA

[2]Department of Climate and Space Sciences and Engineering, University of Michigan, Ann Arbor, MI, 48109, USA

[3]Tomorrow.io, Boston, MA 02210, USA

[4]Center for Hydrometeorology and Remote Sensing, University of California, Irvine, Irvine, CA, USA

[5]Applied Mathematics and Computational Research Division, Lawrence Berkeley National Laboratory, Berkeley, CA, USA

[6]Dept. of Earth and Atmospheric Sciences, Indiana University, Bloomington, IN, USA

[7]Climate and Ecosystem Sciences Division, Lawrence Berkeley National Laboratory, Berkeley, CA, USA

[8]National Weather Service, Western Region Headquarters, Science and Technology Infusion Division, Salt Lake City, UT, USA

[9]Atmospheric Sciences and Global Change Division, Pacific Northwest National Laboratory, Richland, WA, USA
[10]Center for Western Weather and Water Extremes, Scripps Institution of Oceanography, University of California, San Diego, La Jolla, CA, USA
[11]University of Maryland Baltimore County, Baltimore, MD, USA
[12]Global Modeling and Assimilation Office, NASA Goddard Space Flight Center, Greenbelt, MD, USA
[13]Dept. of Land, Air and Water Resources, University of California, Davis, Davis, CA, USA
[14] Department of Civil and Environmental Engineering, The Hong Kong University of Science and Technology, Clear Water Bay, Kowloon, Hong Kong
[15] Department of Geography and Environmental Science, University of Reading, Reading, UK
[16]Joint Institute for Regional Earth System Science and Engineering, University of California, Los Angeles, CA, USA
[17]Dept. of Earth and Planetary Sciences, Yale University, New Haven, CT, USA
[18]Dept. of Meteorology and Atmospheric Science, Pennsylvania State University, University Park, PA, USA
[19] Institute of Meteorology and Climate Research, Karlsruhe Institute of Technology, Karlsruhe, Germany
[20]Universidade de Lisboa, Faculdade de Ciências, Instituto Dom Luiz, Lisboa, Portugal
[21] Instituto Argentino de Nivología, Glaciología y Ciencias Ambientales (IANIGLA-CONICET), Mendonza, Argentina
[22] Department of Civil Engineering, Indian Institute of Technology Madras, Chennai, India

Contents of this file

**Introduction**

IVT and IWV calculations are provided as text. Supplementary figures include coastline mask information and AR occurrences across Tier 1 ARDTs for focus regions including western North America, Europe, and southwestern South America to explain restrictiveness choices and support Figure 3 in main text. Land-only precipitation spread is included to support Figure 4 and precipitation discussion. Supplementary tables include ARDT algorithm details and restrictiveness justification.

**Text S1.**

IVT and IWV are taken from the Tier 1 ARTMIP database and are calculated following Shields et al., 2018.

$$\text{IVT} = -\frac{1}{g}\int_{Pb}^{Pt} (q\boldsymbol{V}_h)\, dp \qquad (1)$$

where q is the specific humidity, $\mathbf{V}_h$ is the horizontal wind vector, Pb is 1000hPa, Pt is 200hPa, and g is the acceleration due to gravity.

$$\text{IWV} = -\frac{1}{g}\int_{Pb}^{Pt} q\, dp \qquad (2)$$

where q is the specific humidity, Pb is 1000hPa, Pt is 200hPa, and g is the acceleration due to gravity.

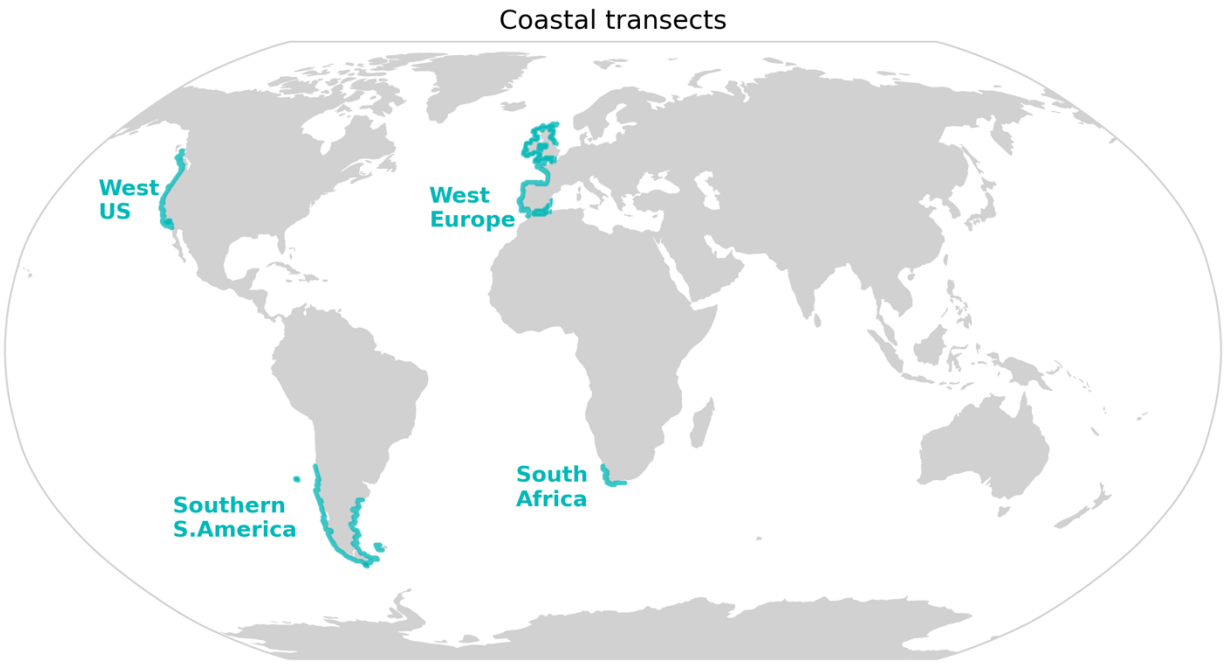


**Figure S1**. Coastal transects for Figure 3 and 4 in the main article. For the Western US and Europe, which includes both UK and Iberian Peninsula, masks are taken from Shields_Kiehl algorithm for direct comparison; for Southern South America and South African coastline points were chosen for consistency with regional Tier 1 ARDT's developed by Viale and Ramos et al., (IDL_v2s), respectively.

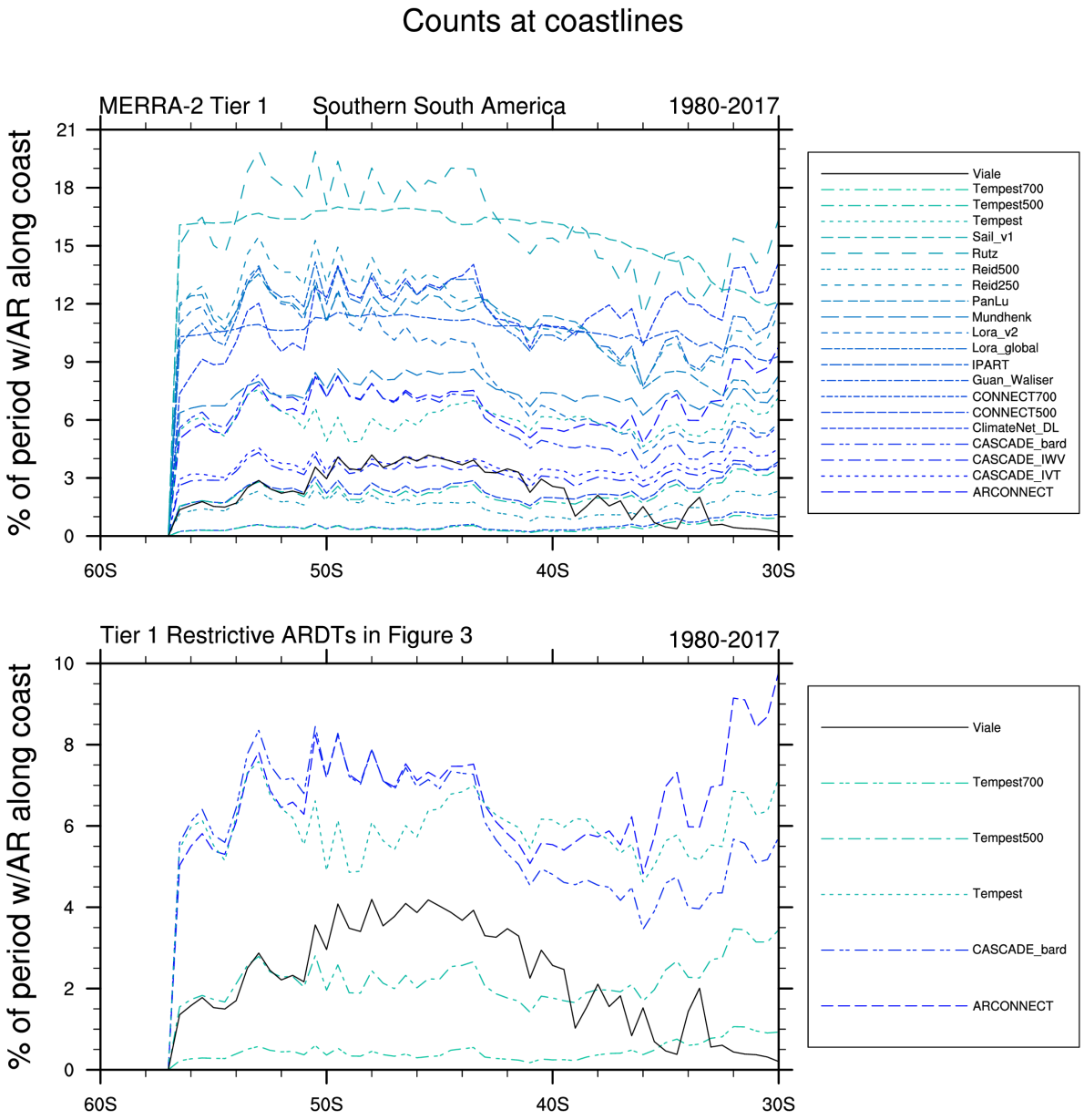


**Figure S2**. South American AR occurrences for the Full Tier 1 ARDT catalogues (a) and only global ARDTS applied to Figure 3i that directly compare Viale regional ARDT (b). One explanation for the subtropical maximum detected by many of the global ARDTs could be the prevalent coastal southern winds trapped by the marine boundary layer. IVT values can exceed the typical ARDT threshold of 250 $kgm^{-1}s^{-1}$ and could potentially be "miscounted" as an AR.

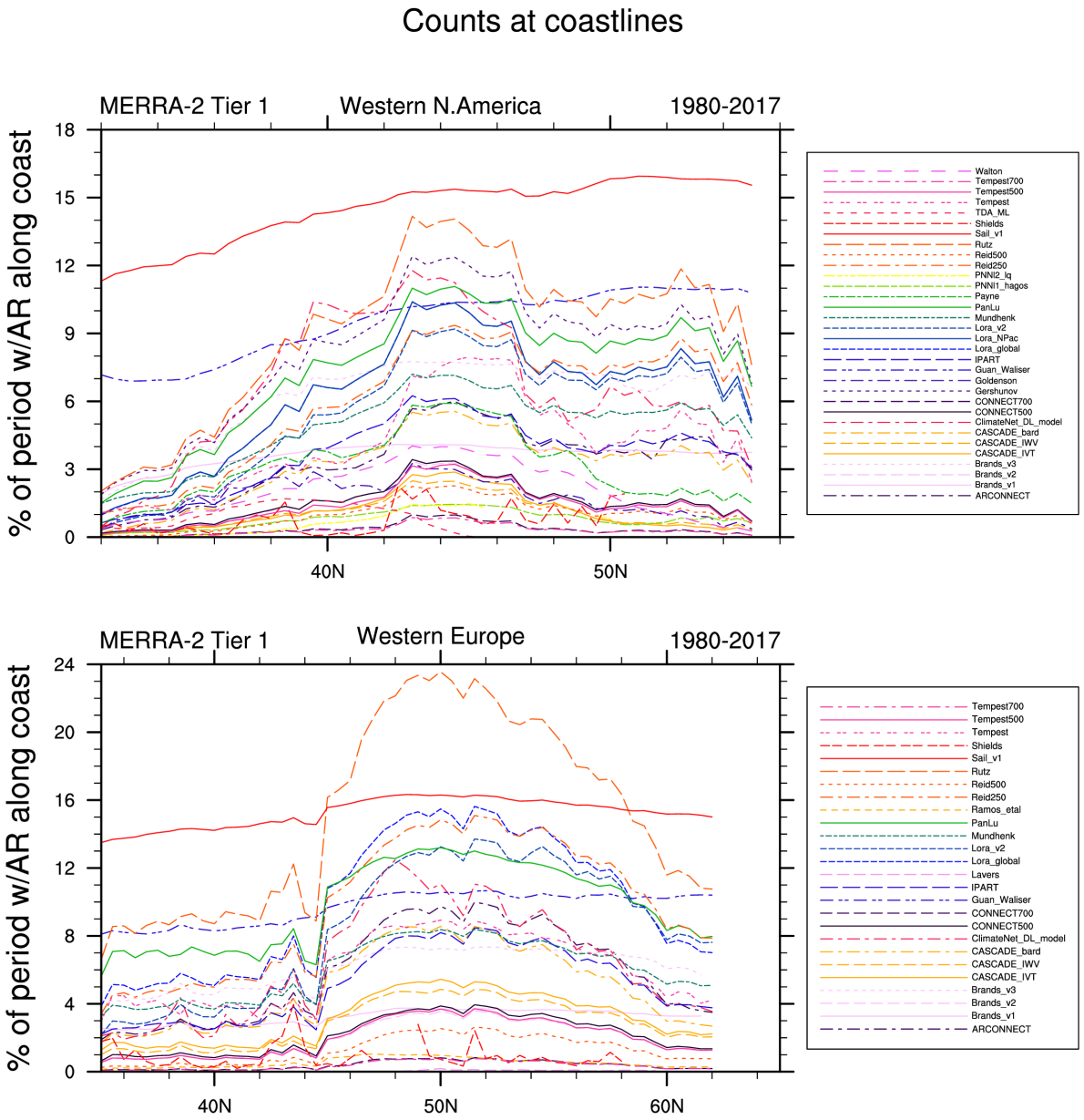


**Figure S3.** Tier 1 AR occurrence metrics by method for Western North America and Western Europe.

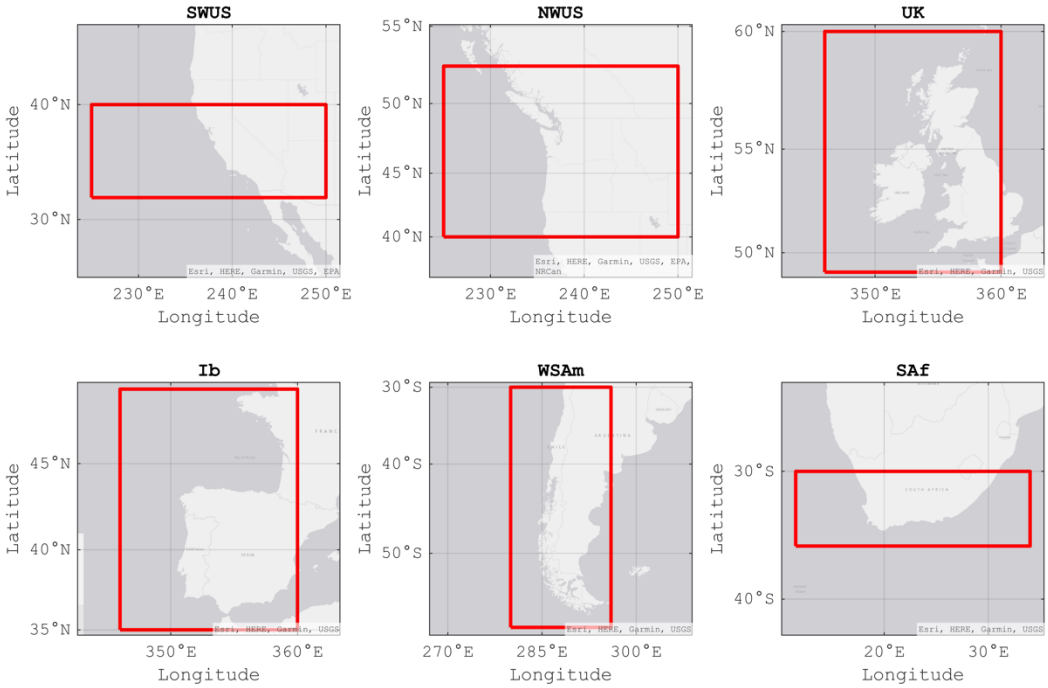


**Figure S4.** Geographic regions for precipitation distributions. All grid points within the red boxes are included in calculations in the main text. Figure S5 includes only land points within the Western U.S. box.

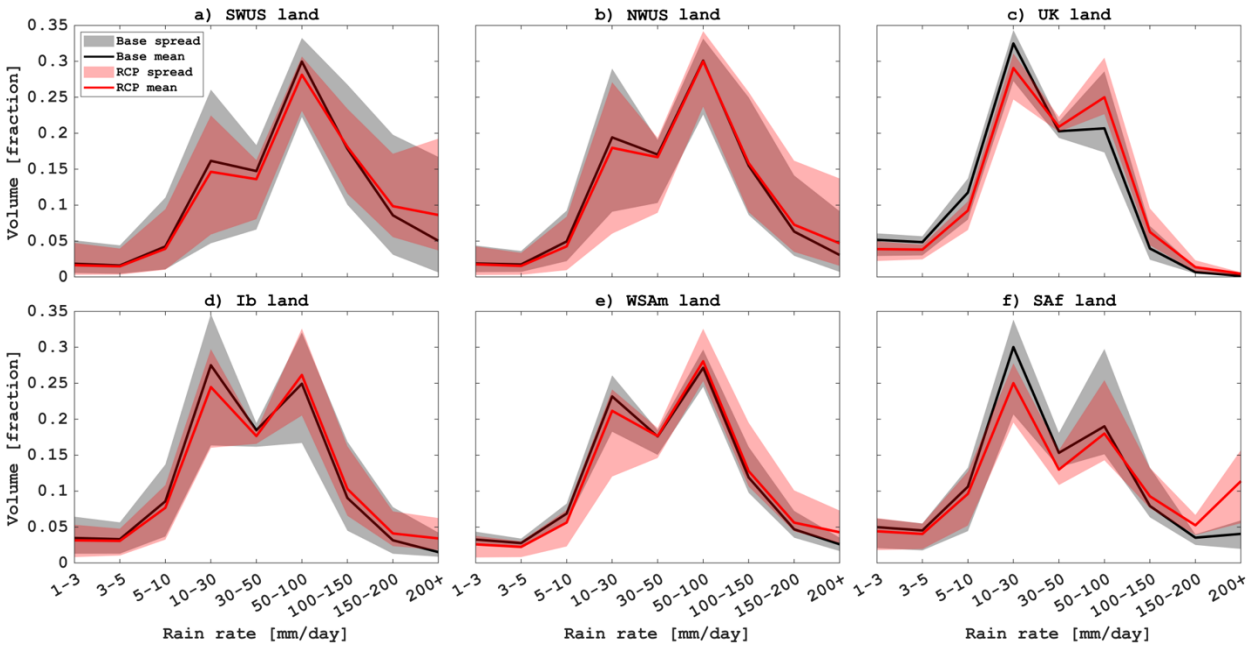


**Figure S5.** Precipitation distribution for land points only across all ARDTs. ARDT mean is shown in heavy bold lines, and the spread in shading. Although the signal is similar to the full regional area (land + ocean), land-only distributions highlight, on the whole, greater uncertainty, and especially so for Western North America.

| ARDT Name/Developer | Region | Algorithm Summary | Restrictiveness | DOI Reference |
|---|---|---|---|---|
| AR-Connect | Global** | Object identification; Absolute: IVT thresholds used = 700 kg/m/s for seeding, 300, for region growing; Time stitching, minimum 24-hour period; Global weighted centroid of AR event must be outside tropics (23.25 N - 23.25 S) | R | 10.1029/2020JD033425 |
| Gershunovetal_2017_v1 | Western North America | >= 1500km long Absolute: 250kgm$^{-1}$s$^{-1}$ IVT; 1.5cm IWV; Time stitching 18 hours | LR | 10.1002/2017GL074175 |
| Goldenson_v1-1 | Western North America | > 2000km long and < 1000km wide Object recognition; Absolute: 2cm IWV | R | 10.1175/JCLI-D-18-0268.1 |
| Guan_Waliser_v2 | Global** | Length >2000km and length width ratio >2; Coherent IVT direction within 45° of AR shape orientation and with a poleward component; Relative: 85th percentile IVT; Absolute min requirement designed for polar locations: 100kg/m/s IVT; Time slice condition | LR | 10.1002/2015JD024257 10.1175/JHM-D-17-0114.1 |
| Ramos et al. (IDL_v2s) | Western Europe**, South Africa* | Detected for reference meridians, length >=1500km (1800km*), latitudinal movement <4.5°N; Relative: IVT 85th percentile (1000-300mb); Time slice, but 18-hour minimum for persistent ARs | R | 10.5194/esd-7-371-2016 10.1175/JHM-D-17-0111.1 |
| Lora_v2 | Global** | Length >= 2000km; Relative/Absolute: IVT 225 kg/m/s above time/latitude dependent threshold using 30-day running mean | LR | 10.1016/j.epsl.2020.116293 |

| | | | | |
|---|---|---|---|---|
| | | and zonal average of IWV; Time slice condition | | |
| Mundhenk_v3 | Global** | >1400km length, aspect ratio 1:4, lat limit >16N/S, axis orientation based on IVT; Relative IVT percentiles and/or anomalies both temporal and spatial; Time slice condition | LR | 10.1175/JCLI-D-15-0655.1 |
| PanLu | Global | 1) Length>2000km; 2) Length-Width ratio>2; 3) sum of turning angle<360; 4) percentage within tropics < 95%; 5) 50% < percentage within tropics < 95% or percentage with IVT direction smaller than 15 degrees <50%; Two relative thresholds. Local threshold: smoothed 85% quantile IVT field using the Gaussian kernel density smoothing technique; regional threshold: the 80% quantile of IVT for all grids within 80N and 80S; Time stitching: last for at least 18 hours | LR | 10.1029/2018WR024407 10.1029/2020GL089477 |
| Payne_Magnusdottir_v1 | Western North America | Length > 1200km, landfalling only Relative: 85th Percentile of maximum IVT (1000-500mb) with reference period time varying; Absolute: IWV >2cm, 850mb wind speed > 10m/s; Time stitching (12-hour minimum) | R | 10.1002/2015JD023586 10.1002/2016JD025549 |
| Payne_Magnusdottir_v2 | Western North America | Same are above except reference period dependent on historical period. | LR | 10.1002/2015JD023586 10.1002/2016JD025549 |

| | | | | |
|---|---|---|---|---|
| PNNL_AR_Hagos | Western North America | Dependent on threshold requirements to determine footprint;> 2000 km long and < 1000 km wide; Absolute: 2cm IWV 10ms-1 wind speed; Time slice | R | 10.1175/JCLI-D-14-00567.1 |
| Shields_Kiehl_v1 | Landfalling ARs for Western North America, Europe, Iberian Peninsula | Ratio 2:1, length to width grid points min 200km length; 850mb wind direction from specified regional quadrants, landfalling only; Relative: spatial anomaly moisture threshold (Zhu and Newell 1998) using IWV; Wind threshold defined by regional 85th percentile 850mb wind magnitudes | R | 10.1002/2016GL069476 10.1002/2016GL070470 |
| Teca_Bard_v1 (Previously called Cascade_Bard_v1) | Global** | Runs 1,024 AR detectors simultaneously. Percentile threshold, minimum area, and filter latitude width are all sampled from a posterior distribution that is designed to optimize global AR counts relative to a dataset of AR counts from a set of experts.; Relative threshold (based on spatial percentile for each timestep); An inverted Gaussian filter is applied at the equator to damp out the ITCZ; Time slice condition | R | 10.5194/gmd-13-6131-2020 |
| TEMPEST (IVT threshold 250) | Global** | Contains both an absolute threshold (typically set at IVT>250 kg/m/s) and a relative threshold (which uses a local Laplacian of IVT, typically set at del^2 IVT < -50k); Laplacian IVT thresholds most effective for widths >1000km; cluster size minimum = 120000km2; Time stitching | R | 10.5194/gmd-10-1069-2017 |

| | | | | |
|---|---|---|---|---|
| | | condition, Global, but latitude >=15° | | |
| TEMPEST (IVT threshold 500) | Global | Same as above except for IVT > 500 kg/m/s | R | 10.5194/gmd-10-1069-2017 |
| TEMPEST (IVT threshold 700) | Global | Same as above except for IVT > 700 kg/m/s | R | 10.5194/gmd-10-1069-2017 |
| Viale | Southwestern South America* | Relative: 85th percentile IVT; Absolute min requirement designed for subtropical locations: 100kgm-1s-1 IVT; a frontal zone intercept or locate south (up to 50 km), i.e., mag. of the horizontal gradient of the 1000-850hPa thickness > 5 m 100 km-1) | R | 10.1175/JHM-D-18-0006.1 |

*Only Tier 1 MERRA-2 available

**Tier 2 CMIP5/6 participant

**Table S1**. ARDTs applied to this study including Tier 2 High Resolution and accompanying Tier ARDT algorithm details. Summaries are also available on the ARTMIP webpage (https://www.cgd.ucar.edu/projects/artmip/algorithms.html). *notation refers to ARDTs where only Tier 1 data was available, but included for context in the South American and South African discussion. ** notation refers to ARDTs that also participated in Tier 2 CMIP5/6 climate change experiments described in O'Brien et al., 2022. Note that all ARTMIP Tier 2 participation is voluntary, hence, the different Tier 2 experiments (Shields et al., 2018) each consist of a unique set of ARDTs. Restrictive algorithms are labelled as "R", and less restrictive "LR".

| **Restrictive Methods** | **Restrictiveness justification** |
|---|---|
| AR-CONNECT | Tier 1 occurrence metrics*; absolute, high IVT values |
| Goldenson_v1-1 | Tier 1 occurrence metrics*; absolute, strict geometry |
| Ramos et al. (IDL_v2s) | Tier 1 occurrence metrics*; relative; regional |
| Payne_Magnusdottir_2016 | Tier 1 occurrence metrics*; relative; regional |
| PNNL_AR_Hagos | Tier 1 occurrence metrics*; absolute strict geometry |
| Shields_Kiehl_v1 | Tier 1 occurrence metrics*; relative spatial; regional |
| TECA_Bard_v1 | Tier 1 occurrence metrics*; relative time independent |
| Tempest_v1_250 | Tier 1 occurrence metrics*; strict relative geometry but low absolute value, could fit into both groupings, behaves similar to others in the restrict group for climate change |
| Tempest_v1_500 | Tier 1 occurrence metrics*; strict relative geometry high absolute value |
| Tempest_v1_700 | Tier 1 occurrence metrics*; strict relative geometry high absolute value |
| Viale | Tier 1 occurrence metrics (Figure 3, main paper) |

| **Less Restrictive Methods** | **Restrictiveness justification** |
|---|---|
| Gershunovetal2017_v1 | Tier 1 occurrence metrics*; low absolute value, light geometry although regional |
| Guan_Waliser_v2 | Tier 1 occurrence metrics*; relative time dependent and historical reference period |
| Lora_v2 | Tier 1 occurrence metrics*, relative and |

| | |
|---|---|
| | absolute constraints; running mean reference |
| Mundhenk_v2 | Tier 1 occurrence metrics*; relative time dependent and historical reference period |
| PanLu | Tier 1 occurrence metrics*; relative |
| Payne_Magnusdottir_2016_v2 | Tier 1 occurrence metrics*; relative time dependent and historical reference period |

**Table S2.** Restrictiveness Justification. *Based on (1) Tier 1 Occurrence Statistics (Figure S3) and (2) reference period for climate change if relative method. If ARDT uses historical data for reference period, a less restrictive label is applied.

**References for Supplemental**

Blamey, R. C., Ramos, A. M., Trigo, R. M., Tomé, R., & Reason, C. J. C. (2018). The Influence of Atmospheric Rivers over the South Atlantic on Winter Rainfall in South Africa, Journal of Hydrometeorology, 19(1), 127-142.

Gershunov, A., Shulgina, T., Ralph, F. M., Lavers, D. A., and Rutz, J. J. (2017), Assessing the climate-scale variability of atmospheric rivers affecting western North America, Geophys. Res. Lett., 44, 7900– 7908, doi:10.1002/2017GL074175.

Guan, B., and D. E. Waliser, (2015). Detection of atmospheric rivers: evaluation and application of an algorithm for global studies. J. Geophys. Res. Atmos., 120, 12, 514–535.

Hagos, S., Leung, L. R., Yang, Q., Zhao, C., & Lu, J. (2015). Resolution and Dynamical Core Dependence of Atmospheric River Frequency in Global Model Simulations, Journal of Climate, 28(7), 2764-2776.

Mundhenk, B. D., E. A. Barnes, and E. D. Maloney (2016). All-season climatology and variability of atmospheric river frequencies over the North Pacific, J. Climate, 29, 4885 4903.

O'Brien, T. A., Risser, M. D., Loring, B., Elbashandy, A. A., Krishnan, H., Johnson, J., Patricola, C. M., O'Brien, J. P., Mahesh, A., Arriaga Ramirez, S., Rhoades, A. M., Charn, A., Inda Díaz, H., & Collins, W. D. (2020). Detection of atmospheric rivers with inline uncertainty quantification: TECA-BARD v1.0.1. Geoscientific Model Development, 13(12), 6131–6148.

Pan, M. and Lu, M. (2019). A Novel Atmospheric River Identification Algorithm, Water Resources Research, 2019, 55: 6069-6087.

Payne, A. E., and Magnusdottir, G. (2015), An evaluation of atmospheric rivers over the North Pacific in CMIP5 and their response to warming under RCP 8.5, J. Geophys. Res. Atmos., 120, 11,173– 11,190, doi:10.1002/2015JD023586.

Payne, A. E., and Magnusdottir, G.(2016), Persistent landfalling atmospheric rivers over the west coast of North America, J. Geophys. Res. Atmos., 121, 13,287– 13,300, doi:10.1002/2016JD025549.

Ramos, A. M., Nieto, R., Tomé, R., Gimeno, L., Trigo, R. M., Liberato, M. L. R., and Lavers, D. A.: Atmospheric rivers moisture sources from a Lagrangian perspective, Earth Syst. Dynam., 7, 371–384, https://doi.org/10.5194/esd-7-371-2016, 2016.

Shearer, E. J., Nguyen, P., Sellars, S. L., Analui, B., Kawzenuk, B., Hsu, K., et al. (2020). Examination of global midlatitude atmospheric river lifecycles using an object-oriented methodology. Journal of Geophysical Research: Atmospheres, 125, e2020JD033425.

Shields, C. A., and Kiehl, J. T. (2016), Simulating the Pineapple Express in the half degree Community Climate System Model, CCSM4, Geophys. Res. Lett., 43, 7767– 7773, doi:10.1002/2016GL069476.

Shields, C. A., and Kiehl, J. T. (2016), Atmospheric river landfall-latitude changes in future climate simulations, Geophys. Res. Lett., 43, 8775– 8782, doi:10.1002/2016GL070470.

Shields, C. A., Rutz, J. J., Leung, L.-Y., Ralph, F. M., Wehner, M., Kawzenuk, B., Lora, J. M., McClenny, E., Osborne, T., Payne, A. E., Ullrich, P., Gershunov, A., Goldenson, N., Guan, B., Qian, Y., Ramos, A. M., Sarangi, C., Sellars, S., Gorodetskaya, I., Kashinath, K., Kurlin, V., Mahoney, K., Muszynski, G., Pierce, R., Subramanian, A. C., Tome, R., Waliser, D., Walton, D., Wick, G., Wilson, A., Lavers, D., Prabhat, Collow, A., Krishnan, H., Magnusdottir, G., and Nguyen, P. (2018). Atmospheric River Tracking Method Intercomparison Project (ARTMIP): project goals and experimental design, *Geosci. Model Dev.,* 11, 2455-2474, https://doi.org/10.5194/gmd-11-2455-2018, 2018.

Skinner, C.B., Lora. J.M. Payne, A. E., Pouslen, C. J., (2020), Atmospheric river changes shaped mid-latitude hydroclimate since the mid-Holocene, Earth and Planetary Science Letters, 541.

Ullrich, P.A. and Zarzycki, C.M., (2017). TempestExtremes: A framework for scale-insensitive pointwise feature tracking on unstructured grids. Geoscientific Model Development, 10(3), pp.1069-1090.

Viale, M., Valenzuela, R., Garreaud, R. D., & Ralph, F. M. (2018). Impacts of Atmospheric Rivers on Precipitation in Southern South America, Journal of Hydrometeorology, 19(10), 1671-1687.

Zhu, Y., and R. E. Newell (1998), A proposed algorithm for moisture fluxes from atmospheric rivers, Mon. Weather Rev., 126(3), 725– 735, doi:10.1175/1520-0493(1998)126<0725:APAFMF>2.0.CO;2.